

# Planar MEMS Van de Graaff Generator

EE245 Project, Fall 2001

Angel V. Peterchev

Department of Electrical Engineering and Computer Science  
University of California, Berkeley

*Abstract*— This paper discusses a MEMS implementation of a planar Van de Graaff generator in a standard MUMPs process. The ability to generate high voltages in autonomous MEMS devices may be useful in various applications such as Smart Dust [1].

## I. INTRODUCTION

MEMS power conversion has been the subject of recent interest. References [2], [3], and [4] address power conversion based on capacitively driven spring-mass structures. Reference [2] uses the resonance of such structures to achieve voltage conversion, while [3] and [4] develop vibration-to-electric power conversion. This paper discusses MEMS power conversion based on mechanical transport of charge analogous to the macro-scale Van de Graaff generator (Fig. 1). The mechanical energy need to achieve the conversion can be supplied by various sources like electrical actuators, micro-combustion engines, vibrations, *etc.*

In a Van de Graaff generator a belt consisting of insulated conductive tiles is positively charged by a voltage source and the charge is delivered to and deposited in a hollow metal sphere (a “dome”) [5]. There, the conductive tiles are charged by another voltage source with a negative charge of the same magnitude as the one they delivered up, and then travel back to ground. As a result positive charge accumulates on the dome yielding potentially very high voltages.

## II. DESIGN

### A. Topology and Analysis of Planar Van de Graaff Generator

Fig. 2 shows a possible topology for a planar Van de Graaff generator. A large capacitor  $C_s$  is used to implement the dome of the generator. Indeed, a parallel-plate capacitor is the 2-D equivalent of the 3-D spherical dome: for a charged conducting sphere all the electric field ( $E_s$ ) is on the outside of the sphere, while for a parallel-plate capacitor the electric field is confined between the two plates [6]. Thus depositing a charge on the inside of the conducting sphere is analogous to depositing charge on the top plate of a parallel-plate capacitor.

The belt of the Van de Graaff generator is implemented with a movable capacitor plate (shuttle). In the beginning of a charging cycle the shuttle forms a capacitor with a grounded plate and is charged by voltage source  $V_c$ . The shuttle is then moved to connect with the top plate of  $C_s$ . There it forms a capacitor  $C_d$  and is charged with negative charge from  $V_d$ , which it then

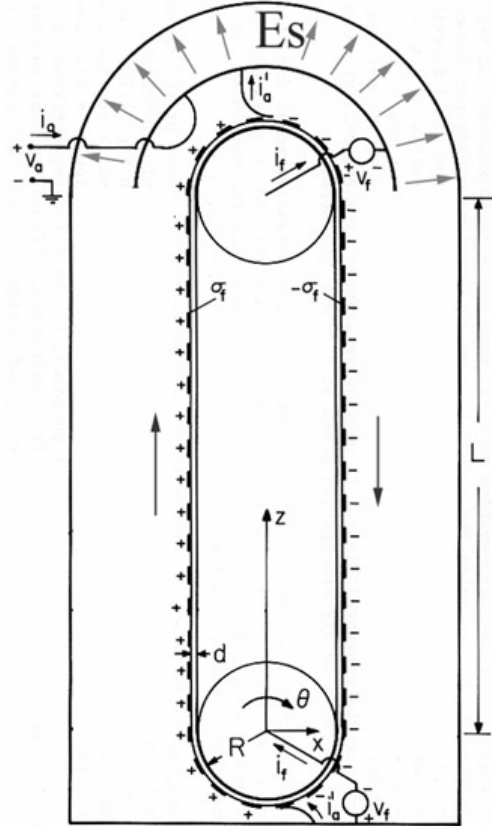


Fig. 1. Diagram of a macro-scale Van de Graaff generator.

returns to ground. The operation of the planar Van de Graaff generator is thus exactly analogous to its 3-D counterpart. The mechanical work done to move the shuttle back and forth over a cycle is ideally (ignoring friction, *etc.*)

$$W_{mech} = 2q_s(V_o - V_c), \quad (1)$$

where we assumed  $C_c = C_d$  and  $V_c = V_d$ , and  $q_s$  is the magnitude of the charge of the shuttle.

The planar Van de Graaff generator is governed by the difference equation

$$\Delta V_o[n] = \frac{C_c + C_p}{C_s} V_c + \frac{C_d}{C_s} V_d - \frac{C_p}{C_s} V_o[n], \quad (2)$$

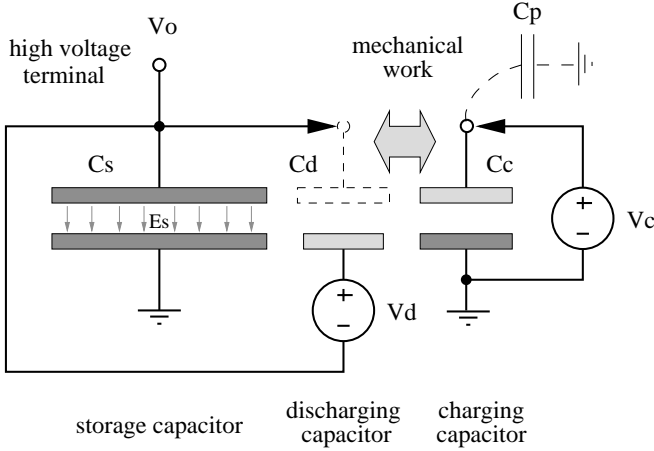


Fig. 2. Principle of planar Van de Graaff generator.

where  $n$  is a discrete time index corresponding to the number of charging cycles completed, and  $C_p$  is parasitic capacitance between the shuttle and ground. Under the assumption that we want to operate the topology in Fig. 2 as a Van de Graaff (high voltage) generator, we have  $V_c = V_d$ ,  $C_c = C_d$ ,  $V_o \gg V_c$ , and  $C_s \gg C_c \gg C_p$ . Then (2) becomes

$$\Delta V_o[n] \approx \frac{2C_c}{C_s} V_c - \frac{C_p}{C_s} V_o[n]. \quad (3)$$

It can be seen that  $C_p \neq 0$  has a detrimental effect on the charge pumping, and the output voltage cannot be increased beyond  $V_{0,max} = 2V_c C_c / C_p$ . Therefore, in a practical design it is desirable to keep  $C_p$  low.

Another interesting case corresponds to  $C_d = 0$ , which is analogous to a Van de Graaff generator without a discharging voltage source in its dome. Then we have

$$\Delta V_o[n] \approx \frac{C_c}{C_s} V_c - \frac{C_p}{C_s} V_o[n], \quad (4)$$

which is comparable to (4), and does not require a floating voltage source attached to the high voltage terminal. The problem, however, is that in a planar implementation of such a scheme it will be very hard to keep  $C_p$  small. To keep  $C_p$  small the movable top plate of  $C_c$  has to be kept away from ground when charging  $C_s$ , which is easy in a 3-D Van de Graaff generator (the dome is high above ground), but difficult in the planar version.

### B. MEMS implementation

A planar Van de Graaff generator prototype was designed in the standard MUMPs process. The MUMPs process [7] is a surface micromachining process with three structural polysilicon layers, two sacrificial oxide layers, and a metal (gold) top layer. The MUMPs layers are summarized in Table I. This process was chosen since it is accessible and the availability of multiple poly layers allows for a direct implementation of

TABLE I  
MUMPS PROCESS SUMMARY

Material Layer	Thickness ( $\mu\text{m}$ )	Symbol
Substrate		SUB
Nitride	$t_{NIT}$	0.6 NIT
Poly 0	$t_{P0}$	0.5 P0
First Oxide	$t_{OX1}$	2.0 OX1
Dimple	$t_{DIMP}$	0.75 DIMP
Poly 1	$t_{P1}$	2.0 P1
Second Oxide	$t_{OX2}$	0.75 OX2
Poly 2	$t_{P2}$	1.5 P2
Metal	$t_M$	0.5 M

TABLE II  
PARAMETER SIZING

Constants		
$\epsilon_0$	permittivity of air	$8.9 \times 10^{-12}$ F/m
$\epsilon_{SiO_2}$	permittivity of the oxides	$4.4\epsilon_0$ (*)
$\epsilon_{Si_3N_4}$	permittivity of the nitride	$4.2\epsilon_0$ (*)
Sizing		
$V_c, V_d$	charging voltages	15 V
$A_{sh}$	shuttle area	$200 \times 200 \mu\text{m}^2$
$C_c, C_d$	shuttle capacitance	0.5 pF
$C_p$	parasitic shuttle capacitance	0.05 pF
$A_{Cs}$	storage cap area	$600 \times 600 \mu\text{m}^2$
$C_s$	storage capacitor	60 pF

(\*) From [9]

the topology on Fig. 2. Further, a metal layer is desirable for the implementation of low-resistance contacts for the shuttle.

Fig. 3 shows the layout of the shuttle, capacitor  $C_c$  and  $C_d$  bottom plates, and the contacts for the shuttle. The shuttle is made of a Poly 1 plate, reinforced with Poly 2. Its sizing and the resulting capacitances are shown in Table II. The size of the shuttle was determined by requiring that  $C_c \gg C_p$  due to the discussion in Section II-A. The main contribution to  $C_p$  comes from the capacitance between the shuttle rails and ground. The rails were shrunk down to the design rule limit of the process, so that  $C_c$  can be minimized which results in small charges being transported and thus low currents in the mechanical contacts. Poly 2 and Metal (gold) implement the contacts needed to connect the shuttle sequentially to  $V_c$  and  $V_o$ . The contacts are modeled after [8]. The need of dynamically switched mechanical contacts in this topology can be a major disadvantage for practical applications. Nevertheless, other topologies that use semiconductor switching may benefit from the principles discussed here.

In the present design the shuttle is not connected to any source of mechanical energy, since this implementation is intended as a proof-of-concept. In practice the shuttle may be connected to devices which generate substantial linear displacements such as inchworm motors [10]. One problem is

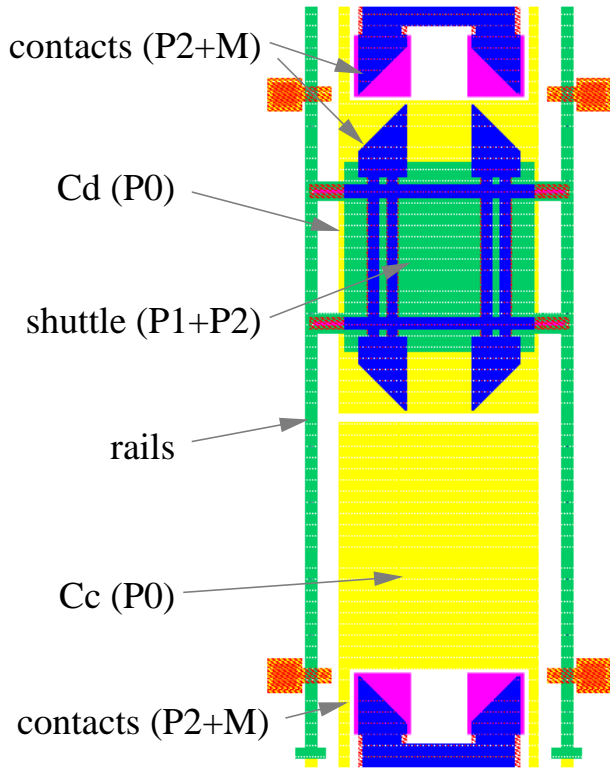


Fig. 3. Layout of shuttle, capacitor  $C_c$  and  $C_d$  bottom plates, and contacts for the shuttle.

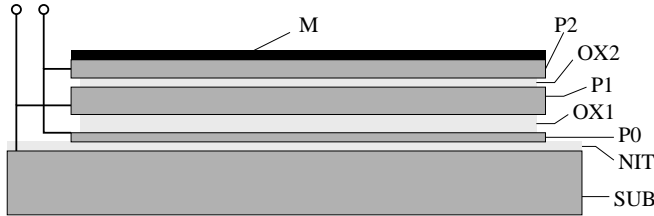


Fig. 4. Implementation of a large capacitor in MUMPs.

providing electrical insulation between the motor and the shuttle (to prevent charge leakage) since the MUMPs structural layers (poly) are conductive. Some hybrid process may have to be used to provide the shuttle insulation. Another possible problem involves the conversion losses associated with the shuttle rail friction.

The storage capacitor  $C_s$  was designed large ( $C_s \gg C_c$ ) so it can provide high peak power at the output of the generator (See Table II). It was implemented using all structural layers as well as the substrate, and making use of the higher permittivity of the oxides and the nitride. Fig. 4 shows a cross-section of  $C_s$ : Poly 1 and the substrate form the bottom plate, while Poly 0 and Poly 2—the top plate. The Dimple mask is used to decrease the distance between Poly 0 and Poly 1, thus increasing

TABLE III  
TEST STRUCTURE DESIGN PARAMETERS

Constants		
$E_P$	Young's modulus for poly	155 GPa
Spring		
$t_b$	beam thickness	$2 \mu\text{m}$
$L_0$	single beam length	$60 \mu\text{m}$
$\alpha$	mult. for comb. of beams	1/12
$K$	spring constant	0.96 N/m
Comb Actuator		
$g$	gap between fingers	$2 \mu\text{m}$
$\beta$	mult. for comb. of fingers	24
$\Delta x$	displacement of comb	$< 10 \mu\text{m}$
$\Delta v$	vernier resolution	$0.25 \mu\text{m}$

capacitance. Continuous vias between the layers on the sides ensure that the capacitor is “sealed” and as a result the release etch will not affect the oxide between the plates which helps achieve high capacitance.

### III. TEST STRUCTURES AND EXPECTED RESULTS

The deflection of a simple spring-comb [11] structure can be used to measure the output voltage of the Van de Graaff generator. Layout of the test structure is shown in Fig. 5, and the design parameters are summarized in Table III. The structure further deploys a vernier scale to measure the displacement of the comb. The design was based on the following equations from basic beam and capacitor theory,

$$K = \alpha \frac{E_P t_b^3 t_{P1}}{L_0^3} \quad (5)$$

$$F = \beta \frac{1}{2} \epsilon_0 V_0^2 \frac{t_{P1} + t_{P2}}{g} \quad (6)$$

$$\Delta x = F/K \quad (7)$$

aiming at a reasonable aspect ratio and small size.

The expected output voltage as a function of the number of charging cycles, and the deflection of the comb actuator as a function of the output voltage are given in Fig. 6. The plots are based on equations (5–7) and the design values in Table II and Table III. It can be seen that for this selection of parameters it takes hundreds of cycles to get  $V_o$  above one hundred volts, which may be inconvenient for manual testing of the prototype. To speed up the charging process for testing purposes,  $V_c$  and  $V_d$ , which are laboratory controlled, may be increased, or the design can be modified to have a smaller output storage capacitor  $C_s$ .

### IV. CONCLUSION

This paper discussed a MEMS implementation of a planar Van de Graaff generator in the standard MUMPs process. This

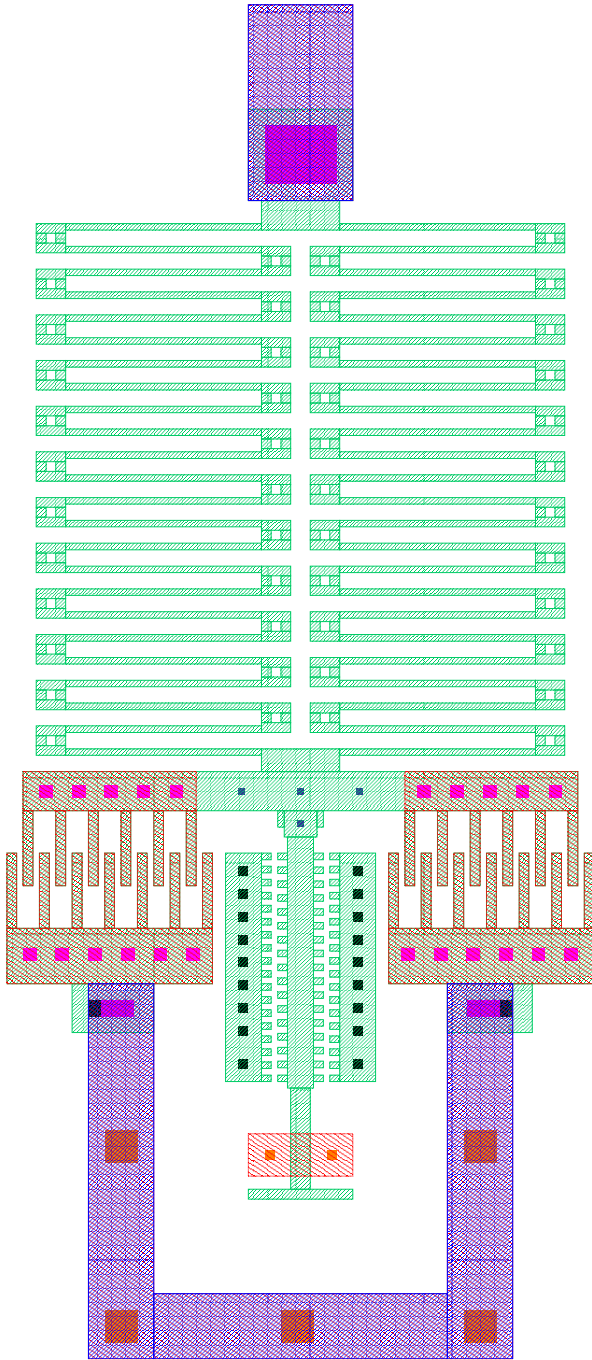


Fig. 5. A spring-gap structure to measure the output voltage of the MEMS Van de Graaff generator.

device achieves power conversion based on mechanical transport of charge. The mechanical energy needed to achieve the conversion can be supplied by various sources like electrical actuators, micro-combustion engines, vibrations, etc. The ability to generate high voltages in autonomous MEMS devices may be useful in various applications such as Smart Dust [1]. The proposed implementation has some significant disadvan-

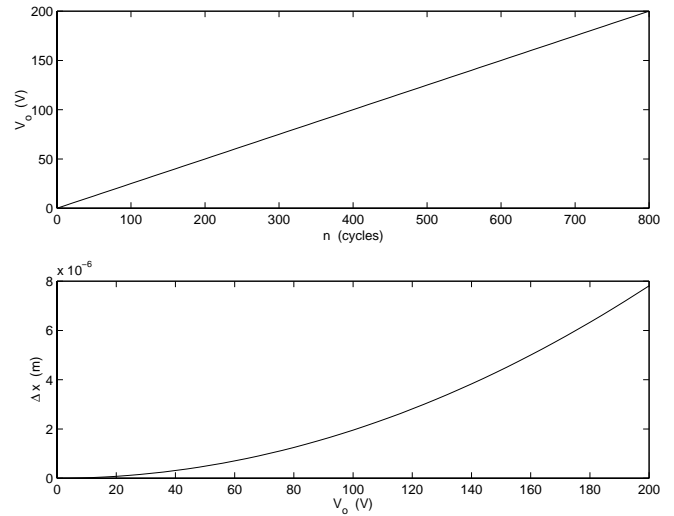


Fig. 6. Relations between number of charge cycles and output voltage, and between output voltage and comb actuator displacement, for the presented planar Van de Graaff generator.

tages such as the dynamic use of electromechanical contacts, the lack of insulating structural layers in MUMPs, and the friction losses from moving the shuttle.

#### REFERENCES

- [1] B. Warneke, M. Last, B. Liebowitz, and K. S. J. Pister, "Smart dust: Communicating with a cubic-millimeter computer," *Computer Magazine*, pp. 44–51, Jan. 2001.
- [2] J. M. Noworolski, "Micromechanical power conversion," Ph.D. dissertation, U.C. Berkeley, April 1998.
- [3] S. Meninger, J. O. Mur-Miranda, R. Amirtharajah, A. Chandrakasan, and J. H. Lang, "Vibration-to-electric energy conversion," *IEEE Trans. on VLSI Systems*, vol. 9, no. 1, pp. 64–76, Feb. 2001.
- [4] R. Amirtharajah, S. Meninger, J. O. Mur-Miranda, A. Chandrakasan, and J. Lang, "A micropower programmable DSP powered using a MEMS-based vibration-to-electric energy converter," in *Proc. ISSCC*, 2000.
- [5] J. R. Melcher, *Continuum Electromechanics*, Cambridge: The MIT Press, 1981.
- [6] J. D. Jackson, *Classical Electrodynamics*, New York: Wiley, third edition, 1998.
- [7] D. A. Koester, R. Mahadevan, B. Hardy, and K. W. Markus, "MUMPs<sup>TM</sup> design handbook revision 6.0," Cronos Integrated Microsystems, <http://www.memsrus.com/cronos/mumps.pdf>.
- [8] E. J. J. Kruglick and K. S. J. Pister, "Lateral MEMS microcontact considerations," *Journal of Microelectronic Systems*, vol. 8, no. 3, pp. 264–71, September 1999.
- [9] D. R. Lide, *CRC Handbook of Chemistry and Physics*, CRC Press, 81<sup>st</sup> edition, 2000-01.
- [10] R. Yeh, S. Hollar, and K. S. J. Pister, "Single mask, large force, and large displacement electrostatic linear inchworm motors," in *Tech. Digest IEEE MEMS*, 2001, pp. 260–4.
- [11] W. C. Tang, T.-C. H. Nguyen, and R. T. Howe, "Laterally driven polysilicon resonant microstructures," in *Proc. IEEE MEMS*, 1989.